Two-dimensional multigap superconductivity in bulk 2*H*-TaSeS

C. Patra, T. Agarwal, Rajeshwari R. Chaudhari, and R. P. Singh *

Department of Physics, Indian Institute of Science Education and Research Bhopal, Bhopal 462066, India

(Received 7 July 2022; revised 10 October 2022; accepted 12 October 2022; published 28 October 2022)

Superconducting transition metal dichalcogenides have emerged as a platform for hosting novel and nontrivial physical phenomena. We report a detailed investigation of superconducting and transport properties on 2*H*-TaSeS single crystals. It suggests that TaSeS is a multigap anisotropic superconductor with the upper critical field, breaking the Pauli limiting field in both in-plane and out-of-plane directions. The angle dependence of the upper critical field suggests the two-dimensional superconducting nature in bulk 2*H*-TaSeS.

DOI: 10.1103/PhysRevB.106.134515

I. INTRODUCTION

Recently, superconductivity in layered transition metal dichalcogenides (TMDs) [1–4] have drawn immense research interest due to its ability to host unique physical properties such as superconductivity, charge density wave (CDW) [5,6], electron-electron correlation [7], and topological properties [8] and can find application in novel electronic, optical, and spintronics devices [9]. TMDs with a general formula MX_2 (M = Mo, W, Ta, Nb and X = Te, Se, S) consist of a layer of TM atoms sandwiched between layers of chalcogen atoms exhibiting generally metallic behavior [10–12] and can exist in different polymorphs such as hexagonal 2*H*, trigonal 1*T*, and rhombohedral 3*R* structures [4,13]. Among the different families of TMDs, archetypal systems, $NbSe_2$ [11], NbS_2 [10], $TaSe_2$ [14], and TaS_2 [15] are reported to be intrinsic superconductors, while superconductivity has been successfully induced by the application of pressure [16–18] and chemical doping in semiconducting MoS_2 [19], $MoSe_2$ [20], and WTe_2 [21].

The Ta-based TMD system, 2*H*-$TaSe_2$ and 2*H*-TaS_2, is known to host charge density wave and superconductivity at low temperatures [22–24]. Moreover, 2*H*-$TaSe_2$ shows CDW ordering at 90 K and the onset of superconductivity at 0.15 K [25,26], and 2*H*-TaS_2 exhibits a chiral charge order system with superconductivity below 0.8 K [23,27]. The enhancement of the superconducting transition in monolayers, pressure, and the intercalation of elements or organic compounds [28–32] resulted from the suppression of CDW by doping or disorder.

Recently, the 4H_b-TaS_2 phase consisted of alternating stacking of weakly coupled 1*T*-TaS_2 (Mott insulator and proposed gapless spin liquid [33]) and 1*H*-TaS_2 [two-dimensional (2D) superconductor with charge density wave] revealed the signature of time-reversal symmetry breaking [34] in the superconducting ground state. Apart from this, the different phase of TaSeS shows exciting superconducting properties. Scanning tunneling microscopic studies on the disorder-driven superconductor 1*T*-TaSeS suggest a nontrivial link between superconductivity and charge order [35,36]. 2*H*-TaSeS shows an enhanced superconducting transition temperature resulting from suppression of the CDW due to disorder, as the similar electronic structure of 2*H*-$TaSe_2$, 2*H*-TaSeS, and 2*H*-TaS_2 ruled out the role of the dopant [24,37]. However, the detailed superconducting, anisotropic, and normal state properties of different phases of TaSeS are not available, which are crucial to understanding the superconducting gap/ground state of any superconductors [24].

In this paper, we report single crystal growth and detailed investigations of electronic and superconducting properties of 2*H*-TaSeS using magnetization, specific heat, and resistivity measurements. It confirms the bulk superconducting transition T_c at 3.90 K. Field- and angle-dependent upper critical field measurements suggest two-dimensional multigap superconductivity breaking the Pauli limiting field. Specific heat measurements also confirm bulk multigap superconductivity in TaSeS.

II. EXPERIMENTAL METHODS

2*H*-TaSeS single crystals were synthesized using the chemical vapor transport method. High-purity (4*N*) Ta, S, and Se, taken in stoichiometric ratios, were thoroughly ground and sealed in a quartz ampoule with iodine (5 mg cm^{-3}) as a transport agent. The ampoule was placed in a two-zone furnace at a temperature gradient of 850 °C–750 °C. After 15 days, shiny single crystals were grown in the cold zone of the tube. The Laue diffraction pattern was recorded using a Photonic-Science Laue camera. The orientation of the crystal plane was also confirmed by x-ray diffraction (XRD) at room temperature on a PANalytical diffractometer equipped with Cu $K\alpha$ radiation (λ = 1.540 56 Å). Magnetization measurements were done using a Quantum Design magnetic measurement system (MPMS3; Quantum Design). Transport properties were measured using the four-probe method and specific heat measurements were performed using the two-tau model in a physical property measurement system (PPMS; Quantum Design).

* rpsingh@iiserb.ac.in

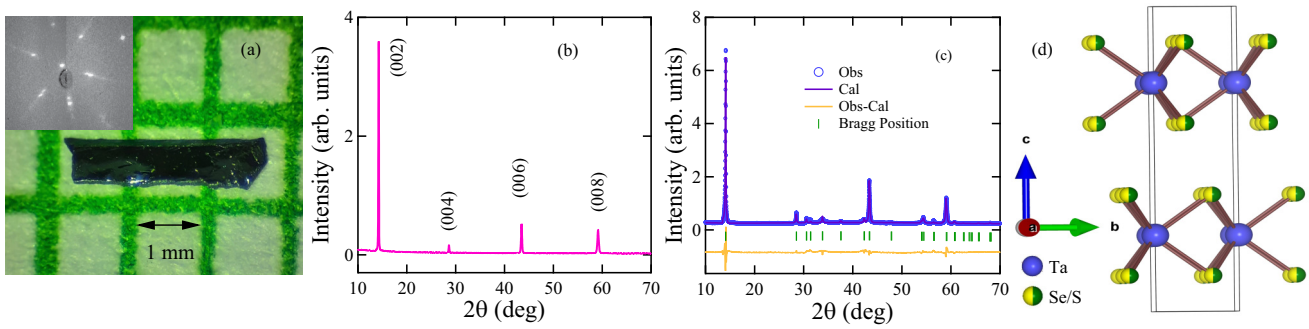

FIG. 1. (a) Shows the microscopic image of the single crystal and the Laue image in the inset. (b) Single crystal powder x-ray diffraction pattern indicates crystal oriented along the [00l] plane. (c) Refinement of powder sample for determining lattice parameters. (d) Side view of 2H-TaSeS unit cell.

III. RESULTS AND DISCUSSION

A. Sample characterization

Figure 1(a) shows the microscopic image of 2H-TaSeS single crystal. The inset of Fig. 1(a) represents the Laue pattern of the crystal and confirms the orientation along the [00l] direction. Powder XRD also confirms the orientation [Fig. 1(b)]. To determine the lattice parameters, powder XRD was performed on crushed single crystals [Fig. 1(c)] and confirmed hexagonal structure with lattice parameters, $a = b = 3.37(2)$ Å, $c = 12.38(4)$ Å, which is consistent with previous reports of 2H-TaS_2 [26]. The unit-cell structure of 2H-TaSeS is shown in Fig. 1(d). The lattice parameters of 2H and 1T phases of TaSeS are tabulated in Table I.

B. Electrical resistivity and magnetization

Resistivity and magnetization measurements have been performed on cleaved crystals (2 mm × 2 mm) from as-grown crystals. The temperature-dependent resistivity of 2H-TaSeS above 10 K, which shows metallic behavior up to 300 K and below 3.905(5) K, undergoes a superconducting transition. The resistivity data above the transition temperature was well fitted by using the Bloch-Grüneisen (BG) model [38–40]. As per this model, resistivity can be described as

$$\rho(T) = \rho_0 + \rho_{BG}(T), \tag{1}$$

where $\rho_{BG}(T)$ is defined as

$$\rho_{BG}(T) = r\left(\frac{T}{\Theta_D}\right)^5 \int_0^{\Theta_D/T} \frac{\Theta_D}{T} \frac{x^5}{(e^x - 1)(1 - e^{-x})} dx, \tag{2}$$

where ρ_0 is the residual resistivity, r is the material-dependent constant, and Θ_D is the Debye constant. The fit using Eq. (1) can be seen in the inset of Fig. 2(a) giving $\rho_0 = 635.42(8)$ $\mu\Omega$ cm, $r = 1.70(2)$ mΩ cm, and $\Theta_D = 115(1)$ K.

From the resistivity measurement, 2H-TaSeS exhibits metallic behavior without containing any CDW signal, whereas the two parent compounds, 2H-TaS_2 and 2H-$TaSe_2$, host both charge density wave and superconductivity [23,26]. Increasing the sulfur or selenium concentration in the parent compounds, CDW is suppressed, and superconductivity is enhanced [24].

The superconducting transition of the sample was confirmed by dc magnetization measurement on a single crystal in zero field cooled warming (ZFCW) and field cooled cooling (FCC) mode with an applied 1 mT field. The transition temperature is observed at $T_c = 3.90(1)$ K for $H \perp c$ [Fig. 2(b)] and $T_c = 3.83(1)$ K for $H \parallel c$. For both perpendicular and parallel field directions, T_c is almost identical.

The lower critical field is extracted from magnetization measurements at constant temperatures. Figure 3(a) represents the field variation of the deviation of isothermal magnetization data from 1.8 to 3.6 K for different directions after subtracting from Meissner lines [41–43]. The lower critical field value for the $H \perp c$ direction is also verified using the method described in [44,45]. The temperature variation of the lower critical field value is fitted with the Ginzburg-Landau

TABLE I. Lattice parameters for 2H-TaSeS and 1T-TaSeS.

Parameter	Unit	2H-TaSeS	1T-TaSeS [14]
Space group		$P63/mmc$	P-3m1
$a = b$	Å	3.37	3.41
c	Å	12.38	6.14
T_c	K	3.90	3.60

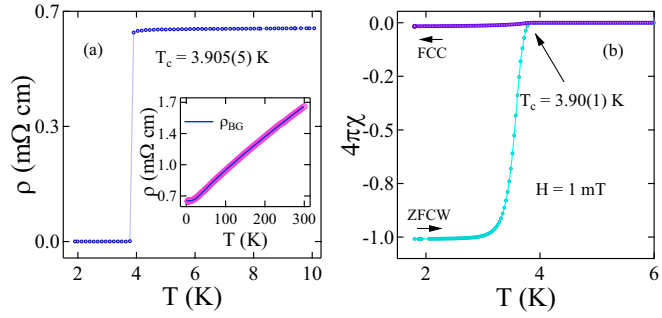

FIG. 2. (a) Zero resistivity drop happens at 3.905(5) K, and the inset shows the resistivity data above the superconducting transition temperature is fitted by the BG model. (b) Magnetization data was collected in ZFCW-FCC mode that shows the superconducting transition temperature at 3.90(1) K at 1 mT applied field.

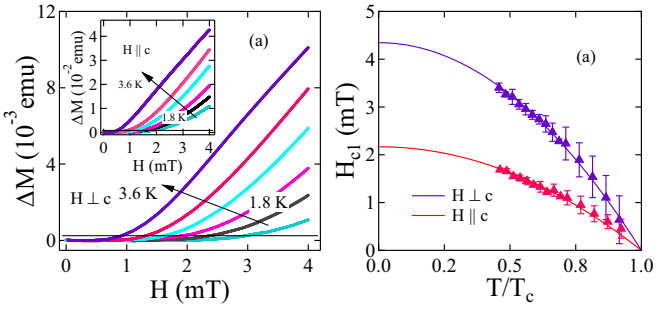

FIG. 3. (a) Low field variation of magnetization data in two different directions. (b) Lower critical field variation with temperature is well fitted with GL equations and gives values 4.3(2) and 2.1(1) mT for $H \perp c$ and $H \parallel c$ directions.

equation by Eq. (3).

$$H_{c1}(T) = H_{c1}(0)\left[1 - \left(\frac{T}{T_c}\right)^2\right]. \tag{3}$$

Figure 3(b) clearly shows anisotropy in a different direction, and the value of $H_{c1}(0)$ for $H \perp c$ is 4.3(2) mT, and for $H \parallel c$ is 2.1 (1) mT.

The upper critical field $[H_{c2}(T)]$ of the 2H-TaSeS system was measured from the transport measurement. The resistivity was measured in both in-plane and out-of-plane directions of the crystal. Figures 4(a) and 4(b) show the resistivity with temperature in different directions in magnetic field up to 6 and 3 T, respectively. From the resistivity curves, $H_{c2}(T)$ values were extracted by taking the onset value of transition temperature for the corresponding field. Figure 4(c) shows the temperature variation of the upper critical field and provides an upturn near T_c in both $H \perp c$ and $H \parallel c$ directions. It cannot be explained by the Ginzburg-Landau theory and the Werthamer-Helfand-Hohenberg [46] model. However, this type of behavior was observed in MgB_2 [47–49], $LaFeAsO_{0.89}F_{0.11}$ [50], and some iron-based superconductors, which can be fitted using the two-band model [51–54]. It can be expressed as

$$\ln\frac{T_c}{T} = \frac{1}{2}\left[U(s) + U(\eta s) + \frac{\lambda_0}{w}\right] - \left\{\frac{1}{4}\left[U(s) - U(\eta s) - \frac{\lambda_-}{w}\right]^2 + \frac{\lambda_{12}\lambda_{21}}{w}\right\}^{1/2},$$
$$H_{c2} = \frac{2\phi_0 T_S}{D_1}; \quad \eta = \frac{D_2}{D_1}, \tag{4}$$

and

$$U(s) = \psi\left(s + \tfrac{1}{2}\right) - \psi\left(\tfrac{1}{2}\right),$$

where $\lambda_- = \lambda_{11} - \lambda_{22}$, $\lambda_0 = (\lambda_-^2 + 4\lambda_{12}\lambda_{21})^{1/2}$, and $w = \lambda_{11}\lambda_{22} - \lambda_{12}\lambda_{21}$. λ_{11} and λ_{22} are the intraband coupling constants, and λ_{12} and λ_{21} are the interband coupling constants. D_1 and D_2 are diffusivities of two bands, respectively. ϕ_0 is flux quantum, and $\psi(x)$ is the digamma function. Figure 4(c) represents the multigap feature with anisotropy in the $H \perp c$ and $H \parallel c$ directions. The fit using Eq. (4) gives the upper critical field value $H_{c2}^{\perp}(0)$ 15.97(3) T for perpendicular and $H_{c2}^{\parallel}(0)$ 9.59(1) T for parallel directions of field.

The Cooper pair can break in the applied magnetic field via the orbital and Pauli paramagnetic limiting in a type-II superconductor. In orbital pair breaking, the field-induced kinetic energy of a Cooper pair exceeds the superconducting condensation energy. In Pauli, paramagnetic limiting is energetically favourable for the electron spins to align with the magnetic field, thus breaking the Cooper pairs. For the type-II superconductor, the Pauli paramagnetic or Clogston-Chandrasekar limit is defined as $H_{c2}^P = 1.86T_c$. The Pauli violation ratio (PVR) is defined as $H_{c2}^{\parallel}(0)/H_{c2}^P$. For 2$H$-TaSeS, PVR in perpendicular and parallel directions are 2.2 and 1.3, respectively. Violation of the Pauli limit of the upper critical field has been observed in other layered superconductors such as $NbSe_2$ [55], NbS_2 [56], and $Ba_6Nb_{11}Se_{28}$ [57], when the applied magnetic field is perpendicular to the crystallographic c axis (see Table II). However, in the case of 2H-TaSeS, this violation has been observed in both in-plane ($H \perp c$) and out-of-plane ($H \parallel c$) directions with an anisotropy factor [$\gamma = H_{c2}^{\perp}(0)/H_{c2}^{\parallel}(0)$] of 1.67 [57–59]. In the layered superconductors, Pauli limit violation can happen due to strong spin-orbit

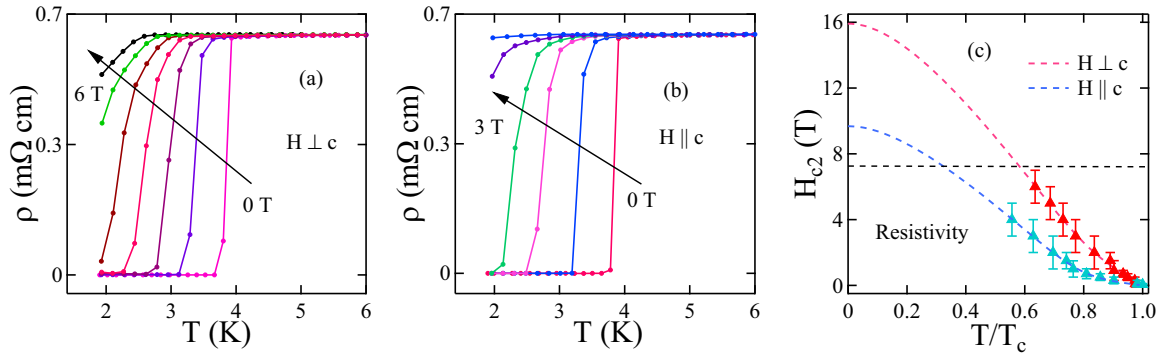

FIG. 4. (a) and (b) Shows resistivity variation with temperature for $H \perp c$ and $H \parallel c$, respectively. (c) The two-gap fitting of the upper critical field from resistivity data for perpendicular and parallel directions and the black dashed line shows the Pauli limit of the upper critical field, i.e., $H_{c2}^P = 1.86T_c = 7.25$ T.

TABLE II. Superconducting parameters for 2*H*-TaSeS with some layered compounds.

Parameter	TaSeS	$NbSe_2$ [55]	NbS_2 [56]	$Ba_6Nb_{11}Se_{28}$ [57]
$H_{c2}^{\perp}$(T)	15.97	17.3		8.84
$H_{c2}^{\parallel}$(T)	9.59	5.3	1.6	0.57
H_{c2}^{P}(T)	7.25	13.54	10.4	4.27
$\xi_{\perp c}$(Å)	58.61	78.8	143	240.4
$\xi_{\parallel c}$(Å)	35.19	24.1	9.7	15.6
γ	1.67	3.3	7.94	10.53

coupling or finite-momentum pairing [60,61]. Strong spin-orbit coupling leads to Ising-type superconductivity, which has recently been observed in the monolayer 2*H*-$NbSe_2$ [62,63]. The finite-momentum pairing can give rise to the Fulde-Ferrell-Larkin-Ovchinnikov (FFLO) state. Further low-temperature angle-dependent measurements and theoretical inputs are required to confirm the exact mechanism of Pauli limit violation.

The resistivity was measured at different angles to explore further the anisotropy, in-plane, and out-of-plane upper critical fields. The angle variation of the field dependence of the resistivity at 2.5 K [64] is shown in Fig. 5(a), where θ is the angle between the magnetic field and the normal to the sample plane. The angle dependence of the resistivity curve shows a clear anisotropy signature from angles $\theta = 0^\circ$ ($H \parallel c$) to $\theta = 90^\circ$ ($H \perp c$). The upper critical field [$H_{c2}(\theta, T)$] data in Fig. 5(b) shows a cusplike peak at $\theta \simeq 90^\circ$. This angular dependence of cusplike feature can be explained by two models, i.e., the three-dimensional (3D) anisotropic GL (AGL) model and the model for thin film, the 2D Tinkham model [65–67]. The relevant equations for these models are in Eq. (5) and Eq. (6), respectively.

$$\left(\frac{H_{c2}(\theta,T)\sin\theta}{H_{c2}^{\perp}}\right)^2 + \left(\frac{H_{c2}(\theta,T)\cos\theta}{H_{c2}^{\parallel}}\right)^2 = 1, \quad (5)$$

$$\left(\frac{H_{c2}(\theta,T)\sin\theta}{H_{c2}^{\perp}}\right)^2 + \left|\frac{H_{c2}(\theta,T)\cos\theta}{H_{c2}^{\parallel}}\right| = 1. \quad (6)$$

The solid orange and green lines show the 3D GL and 2D Tinkham model fitting. The 2D Tinkham model gives a better fit than the others represented in the inset of Fig. 5(b). This

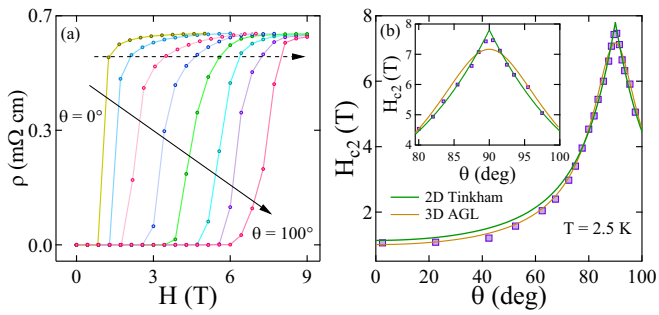

FIG. 5. (a) The angle dependence resistivity variation indicates anisotropy in the system. (b) The angle dependence upper critical field from resistivity measurement 2.5 K fitted with the 3D GL model and the 2D Tinkham model.

implies that the sample is better described by 2D superconductivity than 3D. Similar behavior was observed in 4H_b-TaS_2 [34].

The Ginzburg-Landau coherence length [$\xi_{\perp c}(0) = 58.61(2)$ Å and $\xi_{\parallel c}(0) = 35.19(2)$ Å] is estimated using $H_{c2}^{\parallel c}(0) = \frac{\phi_0}{2\pi\xi_{\perp c}^2(0)}$ and $H_{c2}^{\perp c}(0) = \frac{\phi_0}{2\pi\xi_{\parallel c}(0)\xi_{\perp c}(0)}$. Using the Ginzburg-Landau coherence lengths and the lower critical field values [$H_{c1}^{\perp}(0) = 4.3(2)$ mT and $H_{c1}^{\parallel}(0) = 2.1(1)$ mT], the penetration depth of Ginzburg-Landau [$\lambda_{\perp c}(0) = 6115(13)$ Å and $\lambda_{\parallel c}(0) = 2821(11)$ Å] is calculated using Eqs. (7) and (8) [68].

$$H_{c1}^{\parallel c}(0) = \frac{\phi_0}{4\pi\lambda_{\perp c}^2(0)}\ln\left[\frac{\lambda_{\perp c}(0)}{\xi_{\perp c}(0)} + 0.12\right], \quad (7)$$

$$H_{c1}^{\perp c}(0) = \frac{\phi_0}{4\pi\lambda_{\parallel c}\lambda_{\perp c}(0)}\ln\left[\frac{\lambda_{\parallel c}(0)}{\xi_{\parallel c}(0)} + 0.12\right], \quad (8)$$

where ϕ_0 ($= 2.07 \times 10^{-15}$ T m^2) is the magnetic flux quantum. The two characteristic length parameters are used to calculate the Ginzburg-Landau parameter $\kappa_{\perp c} = 104$ and $\kappa_{\parallel c} = 80 > \frac{1}{\sqrt{2}}$ by Eq. (9), indicating a type-II behavior of the sample.

$$\kappa_{\perp c} = \frac{\lambda_{\perp c}(0)}{\xi_{\perp c}(0)}. \quad (9)$$

C. Specific heat

The zero-field low-temperature specific heat data show a discontinuity at 3.793(5) K, the same as the superconducting transition temperature reported by resistivity and magnetization measurements. The zero-field data above the superconducting transition temperature is fitted with $\frac{C}{T} = \gamma_n + \beta_3 T^2$, where γ_n is the electronic contribution, and β_3 is the phononic contribution. The parameters are 8.13 mJ mol^{-1} K^{-2} and 1.33 mJ mol^{-1} K^{-4}, respectively. Furthermore, the Debye temperature, $\theta_D = 163.34$ K, was calculated using Eq. (10).

$$\theta_D = \left(\frac{12\pi^4 RN}{5\beta_3}\right)^{1/3}, \quad (10)$$

where R is the universal gas constant ($= 8.314$ J mol^{-1} K^{-1}) and N is the number of atoms per formula unit.

To reveal the superconducting gap parameter, the detailed electronic specific heat [$C_{el}(T)$] in the superconducting state is analyzed. The $C_{el}(T)$ [Eq. (12)] in the superconducting state was calculated by subtracting the phononic contribution from total specific heat $C(T)$.

$$C_{el}(T) = C(T) - \beta_3 T^3. \quad (11)$$

The temperature dependence of the electronic contribution of specific heat in the superconducting state can be described using the fully gapped model given in Eq. (12).

$$\frac{S}{\gamma_n T_c} = -\frac{6}{\pi^2}\left(\frac{\Delta(0)}{k_B T_c}\right)\int_0^{\infty}[f\ln(f) + (1-f)\ln(1-f)]dy, \quad (12)$$

where $f(\xi) = \{\exp[E(\xi)/(k_B T)] + 1\}^{-1}$ is the Fermi function $E(\xi) = \sqrt{\xi^2 + \Delta(t)^2}$, where ξ is the energy of the normal electron comparative to the Fermi energy, $y = \xi/\Delta(0)$,

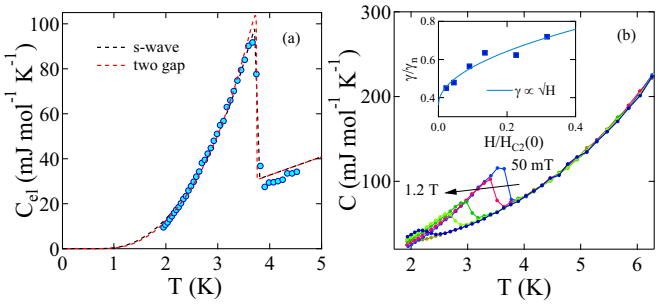

FIG. 6. (a) Low-temperature electronic contribution of specific data is better fitted with a two-gap comparative single-gap model. (b) The Sommerfeld coefficient was calculated from a field-dependent specific heat curve. The inset shows γ depends on the square root of H.

$t = T/T_c$, and $\Delta(t) = \tanh[1.82(1.018[(1/t) - 1])^{0.51}]$ is the BCS approximation for the temperature dependence of the energy gap. The normalized electronic specific heat is related to entropy by Eq. (13).

$$\frac{C_{el}}{\gamma_n T_c} = t\frac{d(S/\gamma_n T_c)}{dt}. \tag{13}$$

The temperature dependence of $C_{el}(T)$ was fitted using Eq. (12) and Eq. (13). In Fig. 6(a), the dotted black line represents the s-wave fitting and gives the gap value of 2.19 meV. It reproduces the experimental data above $T \simeq 2.38$ K. The s-wave fitting deviates at lower temperatures. To explain the temperature behavior, the two-gap phenomenological model α ($s + s$ wave) is used [69–71]. In this model, each band is characterized by the corresponding Sommerfeld coefficient $\gamma_n = \gamma_1 + \gamma_2$, and the total specific heat was calculated by two gap parameters (Δ_1 and Δ_2) and their comparative weights ($\gamma_1/\gamma_n \equiv x$ and $\gamma_2/\gamma_n \equiv 1 - x$). Figure 6(a) (red dotted line) exhibits a better agreement across the whole temperature range, in particular for $T < 2.38$ K. The gap values are 1.49 and 2.27 meV, with a fraction of 0.09. To obtain the true nature of the superconducting gap, heat-capacity data is to be analyzed well below $T_c/10$.

The superconducting gap symmetry can be further confirmed by the magnetic field dependence of the Sommerfeld coefficient $\gamma(H)$. In the type-II fully gapped superconductor, it is proportional to the vortex density. As we apply more field, the vortex density increases because of an increase in field-induced vortices, enhancing the quasiparticle density of states. This gives rise to a linear relation between γ and H, i.e., $\gamma(H) \propto H$ for a nodeless and isotropic s-wave superconductor [72–74]. For a superconductor with nodes in the gap, Volovik predicted a nonlinear relation given by $\gamma(H) \propto \sqrt{H}$ [71,75–77]. The Sommerfeld coefficient γ was calculated by fitting with Eq. (14) for various fields and extrapolating it to $T = 0$ K [see Fig. 6(b)].

$$\frac{C_{el}}{T} = \gamma + \frac{a}{T}\exp\left(-b\frac{T_c}{T}\right). \tag{14}$$

The inset of Fig. 6(b) shows that the Sommerfeld coefficient varies with the square root of H. The linear deviation of γ indicates that TaSeS is a possible multigap system.

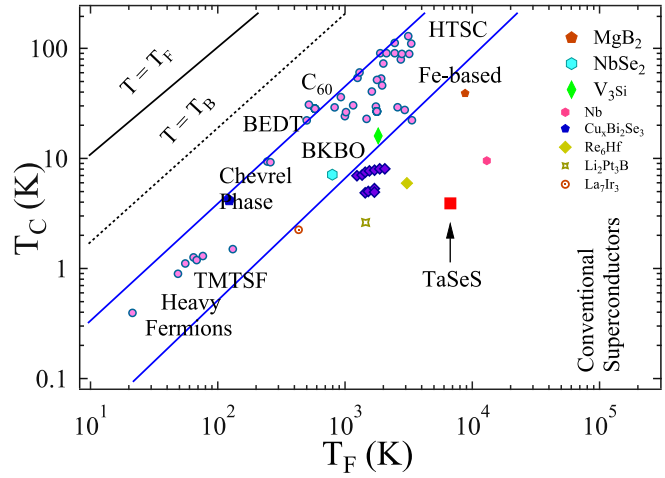

FIG. 7. The plot of the superconducting transition temperature versus the Fermi temperature for different superconducting families. In between, two solid blue lines show the unconventional band of superconductors. TaSeS lies close to the unconventional band.

The fundamental superconducting parameters such as Fermi velocity (v_F), effective mass (m^*), and mean free path (l) are calculated by considering carrier density $n = 2.14 \times 10^{28}$ m^{-3} and $\gamma_n = 8.13$ mJ mol^{-1} K^{-2}. Solving equations from [78] yields $k_F = 0.85 \times 10^{10}$ Å^{-1}, $v_F = 2.04(1) \times 10^5$ m/s, $m^* = 4.86(2)m_e$, and $l = 2.60(1)$ Å. The ratio of coherence length [$\xi_0 \simeq 0.18\frac{\hbar v_F}{k_B T_c} = 721(1)$ Å [79]] and mean free path is $277 \gg 1$, which confirms that $2H$-TaSeS in the dirty limit superconductor.

Superconducting materials can be classified as conventional or unconventional based on the T_c/T_F ratio that was proposed by Uemura *et al.* [80–82]. The known unconventional superconductors, such as Chevrel phases, heavy fermions, high-T_c and Fe-based materials, lie in the range of $0.01 \leqslant T_c/T_F \leqslant 0.1$. In order to classify $2H$-TaSeS, the Fermi temperature T_F has been evaluated by the following equation:

$$k_B T_F = \frac{\hbar^2}{2}(3\pi^2)^{2/3}\frac{n^{2/3}}{m^*}, \tag{15}$$

where n is carrier density 2.14×10^{28} m^{-3} and m^*, effective mass $= 4.86m_e$. The estimated T_F is 6725 K for $2H$-TaSeS and the ratio of $T_c/T_F = 0.0006$ [83–85]. This places $2H$-TaSeS near the band of unconventional superconducting materials (see Fig. 7).

IV. CONCLUSION

In summary, we studied the magnetization, electrical, and magnetotransport properties of $2H$-TaSeS. It confirms multigap superconductivity in $2H$-TaSeS having a superconducting transition temperature of 3.90 K and upper critical field breaking Pauli limit in both the in-plane and out-of-plane directions. The upper critical field angle dependence well fitted with the 2D Tinkham model suggests 2D superconductivity in bulk $2H$-TaSeS single crystals. All results indicate that $2H$-TaSeS is a new candidate for unconventional superconductors

and can host Ising- or FFLO-type superconductivity. Further, low temperature and thickness dependence measurements and theoretical inputs are required to understand the exact superconducting pairing mechanism.

ACKNOWLEDGMENTS

R.P.S. acknowledges Science and Engineering Research Board, Government of India, for the CRG/2019/001028 Core Research Grant.

[1] G. Grüner, Rev. Mod. Phys. **60**, 1129 (1988).

[2] C. J. Arguello, S. P. Chockalingam, E. P. Rosenthal, L. Zhao, C. Gutiérrez, J. H. Kang, W. C. Chung, R. M. Fernandes, S. Jia, A. J. Millis, R. J. Cava, and A. N. Pasupathy, Phys. Rev. B **89**, 235115 (2014).

[3] Z. Wei, B. Li, C. Xia, Y. Cui, J. He, J. B. Xia, and J. Li, Small Methods **2**, 1800094 (2018).

[4] J. C. Meyer, A. K. Geim, M. I. Katsnelson, K. S. Novoselov, T. J. Booth, and S. Roth, Nature (London) **446**, 60 (2007).

[5] A. H. Castro Neto, Phys. Rev. Lett. **86**, 4382 (2001).

[6] J. van Wezel, Phys. Rev. B **85**, 035131 (2012).

[7] H. Zhang and S. C. Zhang, Phys. Status Solidi RRL **7**, 72 (2013).

[8] W.-Y. He, B. T. Zhou, J. J. He, N. F. Q. Yuan, T. Zhang, and K. T. Law, Commun. Phys. **1**, 40 (2018).

[9] X. Zhou, D. Yang, and R. F. Frindtt, J. Phys. Chem. Solids **57**, 1137 (1996).

[10] C. Heil, S. Ponce, H. Lambert, M. Schlipf, E. R. Margine, and F. Giustino, Phys. Rev. Lett. **119**, 087003 (2017).

[11] I. Naik and A. K. Rastogi, Pramana - J. Phys. **76**, 957 (2011).

[12] A. Majumdar, D. VanGennep, J. Brisbois, D. Chareev, A. V. Sadakov, A. S. Usoltsev, M. Mito, A. V. Silhanek, T. Sarkar, A. Hassan, O. Karis, R. Ahuja, and M. Abdel-Hafiez, Phys. Rev. Mater. **4**, 084005 (2020).

[13] G. H. Han, D. L. Duong, D. H. Keum, S. J. Yun, and Y. H. Lee, Chem. Rev. **118**, 6297 (2018).

[14] Y. Liu, R. Ang, W. J. Lu, W. H. Song, L. J. Li, and Y. P. Sun, Appl. Phys. Lett. **102**, 192602 (2013).

[15] S. F. Meyer, R. E. Howard, G. R. Stewart, J. V. Acrivos, and T. H. Geballe, J. Chem. Phys. **62**, 4411 (1975).

[16] Y. Qi, P. G. Naumov, M. N. Ali, C. R. Rajamathi, W. Schnelle, O. Barkalov, M. Hanfland, S. C. Wu, C. Shekhar, Y. Sun, V. Sub, M. Schmidt, U. Schwarz, E. Pippel, P. Werner, R. Hillebrand, T. Forster, E. Kampert, S. Parkin, R. J. Cava *et al.*, Nat. Commun. **7**, 11038 (2016).

[17] M. Mandal, C. Patra, A. Kataria, S. Paul, S. Saha, and R. P. Singh, Supercond. Sci. Technol. **35**, 025011 (2022).

[18] M. Mandal, S. Marik, K. P. Sajilesh, Arushi, D. Singh, J. Chakraborty, N. Ganguli, and R. P. Singh, Phys. Rev. Mater. **2**, 094201 (2018).

[19] R. Zhang, I. L. Tsai, J. Chapman, E. Khestanova, J. Waters, and I. V. Grigorieva, Nano Lett. **16**, 629 (2016).

[20] J. J. Zhang, B. Gao, and S. Dong, Phys. Rev. B **93**, 155430 (2016).

[21] L. Zhu, Q. Y. Li, Y. Y. Lv, S. Li, X. Y. Zhu, Z. Y. Jia, Y. B. Chen, J. Wen, and S. C. Li, Nano Lett. **18**, 6585 (2018).

[22] Y. Kvashnin, D. VanGennep, M. Mito, S. A. Medvedev, R. Thiyagarajan, O. Karis, A. N. Vasiliev, O. Eriksson, and M. Abdel-Hafiez, Phys. Rev. Lett. **125**, 186401 (2020).

[23] V. Vescoli, L. Degiorgi, H. Berger, and L. Forró, Phys. Rev. Lett. **81**, 453 (1998).

[24] L. Li, X. Deng, Z. Wang, Y. Liu, M. Abeykoon, E. Dooryhee, A. Tomic, Y. Huang, J. B. Warren, E. S. Bozin, S. J. L. Billinge, Y. Sun, Y. Zhu, G. Kotliar, and C. Petrovic, npj Quantum Mater. **2**, 11 (2017).

[25] D. C. Freitas, P. Rodiere, M. R. Osorio, E. Navarro-Moratalla, N. M. Nemes, V. G. Tissen, L. Cario, E. Coronado, M. Garcia-Hernandez, S. Vieira, M. Nunez-Regueiro, and H. Suderow, Phys. Rev. B **93**, 184512 (2016).

[26] T. F. Smith, R. N. Shelton, and R. E. Schwall, J. Phys. F: Met. Phys. **5**, 1713 (1975).

[27] J. J. Gao, J. G. Si, X. Luo, J. Yan, Z. Z. Jiang, W. Wang, Y. Y. Han, P. Tong, W. H. Song, X. B. Zhu, Q. J. Li, W. J. Lu, and Y. P. Sun, Phys. Rev. B **102**, 075138 (2020).

[28] M. Abdel-Hafiez, X. M. Zhao, A. A. Kordyuk, Y. W. Fang, B. Pan, Z. He, C. G. Duan, J. Zhao, and X. J. Chen, Sci. Rep. **6**, 31824 (2016).

[29] J. Bekaert, E. Khestanova, D. G. Hopkinson, J. Birkbeck, N. Clark, M. Zhu, D. A. Bandurin, R. Gorbachev, S. Fairclough, Y. Zou, M. Hamer, D. J. Terry, J. J. P. Peters, A. M. Sanchez, B. Partoens, S. J. Haigh, M. V. Milosevic, and I. V. Grigorieva, Nano Lett. **20**, 3808 (2020).

[30] K. E. Wagner, E. Morosan, Y. S. Hor, J. Tao, Y. Zhu, T. Sanders, T. M. McQueen, H. W. Zandbergen, A. J. Williams, D. V. West, and R. J. Cava, Phys. Rev. B **78**, 104520 (2008).

[31] C. S. Lian, C. Heil, X. Liu, C. Si, F. Giustino, and W. Duan, J. Phys. Chem. Lett. **10**, 4076 (2019).

[32] S. Xu, Z. Liu, P. Yang, K. Chen, J. Sun, J. Dai, Y. Yin, F. Hong, X. Yu, M. Xue, J. Gouchi, Y. Uwatoko, B. Wang, and J. Cheng, Phys. Rev. B **102**, 184511 (2020).

[33] K. T. Law and P. A. Lee, Proc. Natl. Acad. Sci. USA **114**, 6996 (2017).

[34] A. Ribak, R. M. Skiff, M. Mograbi, P. K. Rout, M. H. Fischer, J. Ruhman, K. Chashka, Y. Dagan, and A. Kanigel, Sci. Adv. **6**, eaax9480 (2020).

[35] Y. A. Gerasimenko, M. A. Midden, P. Sutar, Z. Jaglicic, E. Zupanic, and D. Mihailovic, arXiv:2109.14585.

[36] Y. A. Gerasimenko, P. Karpov, I. Vaskivskyi, S. Brazovskii, and D. Mihailovic, npj Quantum Mater. **4**, 32 (2019).

[37] G. Y. Guo and W. Y. Liang, J. Phys. C: Solid State Phys. **20**, 4315 (1987).

[38] M. A. Susner, M. Bhatia, M. D. Sumption, and E. W. Collings, J. Appl. Phys. **105**, 103916 (2009).

[39] G. Pristáš, M. Orendáč, S. Gabáni, J. Kačmarčík, E. Gažo, Z. Pribulová, A. Correa-Orellana, E. Herrera, H. Suderow, and P. Samuely, Phys. Rev. B **97**, 134505 (2018).

[40] G. Grimvall, *The Electron-Phonon Interaction in Metals* (North Holland, Amsterdam, 1981).

[41] T. Wang, Y. Ma, W. Li, J. Chu, L. Wang, J. Feng, H. Xiao, Z. Li, T. Hu, X. Liu, and G. Mu, npj Quantum Mater. **4**, 33 (2019).

[42] L. Lyard, P. Szabò, T. Klein, J. Marcus, C. Marcenat, K. H. Kim, B. W. Kang, H. S. Lee, and S. I. Lee, Phys. Rev. Lett. **92**, 057001 (2004).

[43] Z.-C. Wang, Y. Liu, S.-Q. Wu, Y.-T. Shao, Z. Ren, and G.-H. Cao, Phys. Rev. B **99**, 144501 (2019).

[44] M. Abdel- Hafiez, J. Ge, A. N. Vasiliev, D. A. Chareev, J. Van de Vondel, V. V. Moshchalkov, and A. V. Silhanek, Phys. Rev. B **88**, 174512 (2013).

[45] A. Adamski, C. Krellner, and M. Abdel- Hafiez, Phys. Rev. B **96**, 100503(R) (2017).

[46] R. Sultana, P. Rani, A. K. Hafiz, R. Goyal, and V. P. S. Awana, J. Supercond. Novel Magn. **29**, 1399 (2016).

[47] A. Gurevich, S. Patnaik, V. Braccini, K. H. Kim, C. Mielke, X. Song, L. D. Cooley, S. D. Bu, D. M. Kim, J. H. Choi, L. J. Belenky, J. Giencke, M. K. Lee, W. Tian, X. Q. Pan, A. Siri, E. E. Hellstrom, C. B. Eom, and D. C. Larbalestier, Supercond. Sci. Technol. **17**, 278 (2004).

[48] M. S. Park, H. J. Kim, B. Kang, and S. I. Lee, Supercond. Sci. Technol. **18**, 183 (2005).

[49] R. S. Gonnelli, D. Daghero, A. Calzolari, G. A. Ummarino, Valeria Dellarocca, V. A. Stepanov, S. M. Kazakov, N. Zhigadlo, and J. Karpinski, Phys. Rev. B **71**, 060503 (2005).

[50] F. Hunte, J. Jaroszynski, A. Gurevich, D. C. Larbalestier, R. Jin, A. S. Sefat, M. A. McGuire, B. C. Sales, D. K. Christen, and D. Mandrus, Nature (London) **453**, 903 (2008).

[51] N. Kristoffel, T. Ord, and K. Rago, Europhys. Lett. **61**, 109 (2003).

[52] Y. Li, W. Tabis, Y. Tang, G. Yu, J. Jaroszynski, N. Barisić, and M. Greven, Sci. Adv. **5**7349 (2019).

[53] X. Xing, W. Zhou, J. Wang, Z. Zhu, Y. Zhang, N. Zhou, B. Qian, X. Xu, and Z. Shi, Sci. Rep. **7**, 45943 (2017).

[54] I. I. Mazin, O. K. Andersen, O. Jepsen, O. V. Dolgov, J. Kortus, A. A. Golubov, A. B. Kuz'menko, and D. van der Marel, Phys. Rev. Lett. **89**, 107002 (2002).

[55] F. Soto, H. Berger, L. Cabo, C. Carballeira, J. Mosqueira, D. Pavuna, P. Toimil, and F. Vidal, Phys. C (Amsterdam, Neth) **460-462**, 789 (2007).

[56] K. Onabe, M. Naito, and S. Tanaka, J. Phys. Soc. Jpn. **45**, 58 (1978).

[57] K. Ma, S. Jin, F. Meng, Q. Zhang, R. Sun, J. Deng, L. Chen, L. Gu, G. Li, and Z. Zhang, Phys. Rev. Mater. **6**, 044806 (2022).

[58] J. Murphy, M. A. Tanatar, D. Graf, J. S. Brooks, S. L. Budko, P. C. Canfield, V. G. Kogan, and R. Prozorov, Phys. Rev. B **87**, 094505 (2013).

[59] S. Khim, B. Lee, K. Y. Choi, B. G. Jeon, D. H. Jang, D. Patil, S. Patil, R. Kim, E. S. Choi, S. Lee, J. Yu, and K. H. Kim, New J. Phys. **15**123031 (2013).

[60] T. Coffey, C. Martin, C. C. Agosta, T. Kinoshota, and M. Tokumoto, Phys. Rev. B **82**, 212502 (2010).

[61] Y. Cao, J. M. Park, K. Watanabe, T. Taniguchi, and P. J. Herrero, Nature (London) **595**, 526 (2021).

[62] X. Xi, Z. Wang, W. Zhao, J. Park, K. T. Law, H. Berger, L. Forro, J. Shan, and K. F. Mak, Nat. Phys. **12**, 139 (2016).

[63] J. M. Lu, O. Zheliuk, I. Leermakers, N. F. Q. Yuan, U. Zeitler, K. T. Law, and J. T. Ye, Science **350**, 1353 (2015).

[64] Y. J. Sato, F. Honda, Y. Shimizu, A. Nakamura, Y. Homma, A. Maurya, D. Li, T. Koizumi, and D. Aoki, Phys. Rev. B **102**, 174503 (2020).

[65] R. C. Morris, R. V. Coleman, and R. Bhandari, Phys. Rev. B **5**, 895 (1972).

[66] S. Kittaka, T. Nakamura, Y. Aono, S. Yonezawa, K. Ishida, and Y. Maeno, Phys. Rev. B **80**, 174514 (2009).

[67] D. Shen, C. N. Kuo, T. W. Yang, I. N. Chen, C. S. Lue, and L. M. Wang, Commun. Mater. **1**, 56 (2020).

[68] M. Kończykowski, C. J. van der Beek, M. A. Tanatar, V. Mosser, Y. J. Song, Y. S. Kwon, and R. Prozorov, Phys. Rev. B **84**, 180514(R) (2011).

[69] W. L. McMillan, Phys. Rev. **167**, 331 (1968).

[70] M. E. Zhitomirsky and V. H. Dao, Phys. Rev. B **69**, 054508 (2004).

[71] C. L. Huang, J. Y. Lin, Y. T. Chang, C. P. Sun, H. Y. Shen, C. C. Chou, H. Berger, T. K. Lee, and H. D. Yang, Phys. Rev. B **76**, 212504 (2007).

[72] Y. Wang, J. S. Kim, G. R. Stewart, P. J. Hirschfeld, S. Graser, S. Kasahara, T. Terashima, Y. Matsuda, T. Shibauchi, and I. Vekhter, Phys. Rev. B **84**, 184524 (2011).

[73] C. Caroli, P. G. de Gennes, and J. Matricon, Phys. Lett. **9**, 307 (1964).

[74] P. G. de Gennes, *Superconductivity of Metals and Alloys* (W. A. Benjamin, New York, 1966).

[75] N. B. Kopnin and G. E. Volovik, Phys. Rev. Lett. **79**, 1377 (1997).

[76] K. Izawa, A. Shibata, Y. Matsuda, Y. Kato, H. Takeya, K. Hirata, C. J. van der Beek, and M. Konczykowski, Phys. Rev. Lett. **86**, 1327 (2001).

[77] N. Nakai, P. Miranovic, M. Ichioka, and K. Machida, Phys. Rev. B **70**, 100503(R) (2004).

[78] Arushi, D. Singh, P. K. Biswas, A. D. Hillier, and R. P. Singh, Phys. Rev. B **101**, 144508 (2020).

[79] A. Devarakonda, H. Inoue, S. Fang, C. O. Keskinbora, T. Suzuki, M. Kriener, L. Fu, E. Kaxiras, D. C. Bell, and J. G. Checkelsky, Science **370**, 231 (2020).

[80] Y. J. Uemura, V. J. Emery, A. R. Moodenbaugh, M. Suenaga, D. C. Johnston, A. J. Jacobson, J. T. Lewandowski, J. H. Brewer, R. F. Kiefl, S. R. Kreitzman, G. M. Luke, T. Riseman, C. E. Stronach, W. J. Kossler, J. R. Kempton, X. H. Yu, D. Opie, and H. E. Schone, Phys. Rev. B **38**, 909(R) (1988).

[81] Y. J. Uemura *et al.*, Phys. Rev. Lett. **62**, 2317 (1989).

[82] Y. J. Uemura, L. P. Le, G. M. Luke, B. J. Sternlieb, W. D. Wu, J. H. Brewer, T. M. Riseman, C. L. Seaman, M. B. Maple, M. Ishikawa, D. G. Hinks, J. D. Jorgensen, G. Saito, and H. Yamochi, Phys. Rev. Lett. **66**, 2665 (1991).

[83] D. Singh, K. P. Sajilesh, S. Marik, A. D. Hillier, and R. P. Singh, Phys. Rev. B **99**, 014516 (2019).

[84] D. D. Castro, S. Agrestini, G. Campi, A. Cassetta, M. Colapietro, A. Congeduti, A. Continenza, S. D. Negri, M. Giovannini, S. Massidda, M. Nardone, A. Pifferi, P. Postorino, G. Profeta, A. Saccone, N. L. Saini, G. Satta, and A. Bianconi, Europhys. Lett. **58**, 278 (2002).

[85] E. F. Talantsev, Condensed Matter **4**, 83 (2019).